A surface science compatible epifluorescence microscope for inspection of samples under ultra high vacuum and cryogenic conditions

Christian Marquardt,[1] Alexander Paulheim,[1] Nils Rohbohm,[1] Rudolf Merkel,[2] and Moritz Sokolowski[1]

[1]*Institut für Physikalische und Theoretische Chemie der Universität Bonn Wegelerstrasse 12, 53115 Bonn, Germany*

[2]*Institute of Complex Systems, ICS-7: Biomechanics, Forschungszentrum Jülich GmbH, 52425, Germany*

Abstract

We modified an epi-illumination light microscope and mounted it to an ultrahigh vacuum chamber for investigating samples used in a surface science experiment. For easy access and bake out, all optical components are placed outside the vacuum and the sample is imaged through a glass window. The microscope can be operated in reflection brightfield or epifluorescence mode to image the sample surface or fluorescent dye molecules adsorbed on it. The homemade sample mounting was made compatible for the use under the microscope; sample temperatures as low as 6 K can be achieved. The performance of the microscope is demonstrated on two model samples: Brightfield-images of a well prepared Ag(100) surface show a macroscopic corrugation of the surface, although low energy electron diffraction data indicate a highly ordered crystalline surface. The surface shows macroscopic protrusions with flat regions, about 20 – 200 µm in diameter, in between. Fluorescence images of diluted 3,4,9,10-perylene tetracarboxylicacid dianhydride (PTCDA) molecules adsorbed on an ultrathin epitaxial KCl film on the Ag(100) surface show a shading effect at surface protrusions due to an inclined angle of incidence of the PTCDA beam during deposition. For some preparations the distribution of the fluorescence intensity is inhomogeneous and shows a dense network of bright patches about 5 µm in diameter related to the macroscopic corrugation of the surface. We propose that such a light microscope can aid many surface science experiments, especially those dealing with epitaxial growth or fluorescent materials.

Keywords: light microscopy, surface morphology, UHV, cryogenic temperatures

Prepared for Review of Scientific Instruments

I. Introduction

When talking about microscopy in the field of surface science, most people think about scanning probe microscopy[1, 2] (SPM), low energy electron microscopy[3] (LEEM), or photoemission electron microscopy[4] (PEEM). Whereas SPM techniques are best suited for imaging surface areas in the range between a few nm and several 100 nm on the lateral scale with up to atomic resolution,[5] LEEM and PEEM can be used to image surface areas on a mesoscopic scale between a few μm and several 100 μm with up to a few nm resolution.[6, 7] For a larger scale, light microscopy (LM) is the method of choice. However, up to today there is less than a handful of publications describing the use of LM for samples under ultra-high vacuum (UHV) conditions.[8, 9] This is astonishing since LM can be performed in various modes yielding complementary information: Besides brightfield or darkfield imaging for investigations of the sample morphology, also fluorescence- and polarization microscopy can be applied. With the latter techniques, the positions and orientations of isolated or aggregated dye molecules can be determined,[10] giving one the opportunity to study and control thin film growth, nucleation, and phase transitions of the related materials under surface science conditions. Moreover, LM is capable of detecting single molecules and hence gives one the opportunity to study single molecule dynamics and distributions.[8, 9, 11] We note that earliest experiments on organic molecular beam deposition on single crystal surfaces were done by LM, although only *ex-vacuo*.[12]

Most experimental groups that use both surface science techniques and LM perform the sample preparation and first experimental investigations inside the vacuum. The LM is performed outside the vacuum.[13-15] This is extra time consuming and can lead to contamination, modification, or decomposition of the prepared samples. An *in-vacuo* solution would therefore be desirable. However, the design of an UHV compatible light microscope is not trivial: First, it has to fulfill the requirements for UHV operation, which are low outgassing rates and bake out stability so that pressures down to 1×10^{-10} mbar can be achieved. Secondly, it should have ideal illumination and imaging properties as well as flexibility in the use of different objectives and filters. For the design of such a microscope the major problem is the short working distance between the front lens of the microscope objective and the sample surface that is usually less than a millimeter already for medium magnification microscope objectives (20×, 40×). Blumfeld et al. constructed a confocal laser-scanning microscope.[8] They chose an approach with a custom-made vacuum compatible and bakeable Schwarzschild microscope objective placed *inside* the UHV. They were able to image single molecule fluorescence on var-

ious substrates with near-diffraction-limited resolution. However, due to the placement of the microscope objective inside the UHV, they had to accept a maximum bake out temperature of only 100 °C and the risk of a deterioration of the microscope objective.

In this paper, we report on a different and in some aspects more flexible approach to an UHV microscope. It is based on a standard wide field (non-confocal) microscope, which is able to image large sample areas in brightfield or fluorescence mode. It was adapted to an existing surface science setup. This adaption had to fulfill the following aspects: (a) the sample preparation and observation have to be performed under UHV conditions, (b) for higher flexibility and bake out stability all optical components (including the microscope objective) have to be mounted outside the vacuum, (c) the sample has to be easily accessible both by the microscope and other surface science techniques, (d) the sample has to be cold for fluorescence imaging, and (e), this is special to our setup, the microscope has to be retractable from the pathway of the sample in order to grant a transition of the sample into a glass head at one end of the UHV chamber (cf. Fig. 1, below).

In the following Sec. II, the design of the microscope and the sample mounting will be described in detail. In Sec. III we demonstrate the performance of the microscope on a well prepared clean Ag(100) surface for brightfield application and on diluted organic dye molecules adsorbed on a thin KCl film on this surface for fluorescence imaging.

II. System Design

A. UHV system

The microscope was implemented onto a horizontal tube attached to a typical stainless steel UHV chamber, which was equipped with an instrument for spot profile analysis low energy electron diffraction (SPA-LEED, Omicron NanoTechnology GmbH) and designed for fluorescence spectroscopy on organic molecules adsorbed on thin films. The chamber contained a sputter gun for surface preparation and homemade Knudsen-type thermal evaporators for the deposition of alkalihalides and organic molecules. For deposition control, a quadrupole mass spectrometer and quartz-microbalances were used. The Ag(100) sample was invariably mounted on a homemade sample mounting on a horizontal long travel manipulator with a liquid helium cryostat (VAb GmbH). Sample temperatures between 6 K and 1000 K were achieved. (We will report the details of the sample mounting in Sec. II.D.) Structural characterization of the sample was typically done by the SPA-LEED apparatus. For fluorescence spectroscopy, the sample could be transferred into a glass head at the end of the same horizon-

tal tube, to which the microscope was attached. A schematic view of the microscope is shown in Fig. 1.

B. Microscope

The microscope was mounted on a stainless steel UHV 6 way cross (microscope adapter) with a length of 160 mm and an inner diameter of 70 mm. It was inserted between the preparation part of the vacuum chamber and the glass head with two conflat flanges (CF 100, CF 63) and had four additional CF 40 flanges on diametrically opposed sides of the tube (top, bottom, front and back). The flanges in front and back were used as viewports. The flange at the bottom was used for a linear motion feedthrough holding a post, which could stabilize the sample against vibrations. The microscope itself was mounted to the top flange.

As mentioned above the most critical problem concerning the design of an UHV microscope was the required small working distance between the front lens of the microscope objective and the sample. Since the sample was inside the vacuum and in our approach all optical components were supposed to be outside the vacuum, the sample needed to be imaged through a glass window. For mechanical stability and pressure stability, this window had to exhibit a significant thickness. We used a plane borosilicate window (Borofloat 33, Schott AG) with a diameter of 36 mm and a thickness of 1.75 mm. This thickness was indeed below that of conventional UHV windows of similar size (~3 mm), but it still exceeded the typical working distances of medium magnification microscope objectives (20×, 40×). Therefore, we used microscope objectives with larger working distances (details see Sec. II.C.). Optically the window acted as an additional plane parallel plate, i.e. like a thick cover glass slip. We did not use an anti-reflection coating on the glass window so far. This may reduce stray light and increase the detection efficiency. However until now stray light has not been an issue.

To bring the window as close as possible to the sample, it was melted to the foremost end of a glass tube that pointed into the UHV (see Fig. 1). The glass tube had a length of 230 mm, a wall thickness of 2 mm and an inner diameter of 32 mm. At its upper end, it turned into a U-turn before it was connected with a metal glass joint on top of a CF40 flange. This construction may appear laborious, but had a very simple reason: The metal glass joint can only stand compressive but not tensile forces. This was taken into account by orienting the metal glass joint pointing to the high-pressure side in combination with a U-turn made out of glass. The described construction withstood pumping to vacuum and bake out temperatures of at least 150 °C.

To retract the glass tube out of the pathway of the sample, it was mounted to a 50 mm linear transfer (VG Scienta) on the top flange of the microscope adapter. For microscope operation the front window of the glass tube can be approached very close to the sample surface, while watching this from a horizontal window of the microscope adapter at 90°. A drawback of the linear transfer was the elongation of the length of the glass tube, which added to the optical paths of the microscope. Therefore, this option for retraction may be reconsidered if it is not required.

The optical parts of the microscope were connected to the UHV-part via a mounting platform with a circular dovetail. The microscope objective was mounted at the end of a brass tube (see Fig. 1) that fitted inside the glass tube and positioned the objective close to the window at the front end. To avoid stray light, the brass tube was black oxidized at the in- and outside. It had an outer diameter of 30 mm, a wall thickness of 2 mm and a length of 230 mm to compensate the length of the glass tube. The mounting platform was moved and fastened on four 200 mm M8 threaded rods that were attached at the top flange of the linear transfer. By moving the platform on the rods, the distance between the microscope objective and the window at the end of the glass tube could be adjusted. For increase of stiffness and reduction of vibrations, an additional platform was fixed on half way of the rods. The platforms and all optical components could easily be removed for bake out or maintenance. Please note that most conventional microscope objectives typically cannot stand temperatures higher than ~50 °C. Therefore the possibility to remove the objective from the apparatus during bake out was essential.

C. Microscope optical setup

In principle any modular incident light microscope could be used in combination with the above described microscope adapter. We used the *universal epi illuminator* of a Nikon *Optiphot-Pol* microscope and the associated trinocular head for illumination and observation, respectively. The microscope used an incident light Köhler illumination[16] that was designed for a finite tube length of 210 mm. However, due to the elongated glass tube, the nominal standard tube length of 210 mm was exceeded by far (by about 200 mm). To retain ideal Köhler illumination we thus inserted a telescope optics (elongation length 4f) with two achromatic lenses inside the brass tube. The lenses were arranged in such way (distance = 2f, f = 50 mm) that the image plane of the aperture diaphragm was projected into the rear focal plane of the objective and the image plane of the field diaphragm was projected onto the sample. The corresponding conjugated image planes were drawn in Fig. 1. For imaging, a series of *Nikon M Plan* microscope objectives (5× NA 0.1, 10× NA 0.25 and 20× NA 0.4) corrected for a finite

tube length of 210 mm was used. The 20× microscope objective exhibited an extra long working distance (ELWD) so that the thickness of the glass window could be easily tolerated and the front surface of the window was at a minimum distance of 2-3 mm from the surface of the sample. We note that none of the Nikon objectives was corrected for the 1.75 mm thickness of the glass window, which caused some loss of image quality and fluorescence intensity due to spherical aberrations. These issues became more pronounced with increasing NA of the microscope objectives. Therefore, at higher magnification and NA an *Olympus CDPlan 40 PL* objective (40× NA 0.5) was used. This objective exhibits a larger working distance and is equipped with a correction collar, which we used to compensate the effect of the thickness of the glass window (up to 2 mm). Since this objective was corrected for a finite tube length of only 160 mm, and the trinocular head of the microscope exceeded this distance by 50 mm, it was replaced by a shorter homemade adapter tube for the use of this objective. We note that the maximum diameter of all used microscope objectives was 29 mm so that they all fitted smoothly into the glass tube. For detection we used a monochrome, thermoelectrically cooled 12-bit CCD-camera (PCO *Sensicam*) mounted to commercially available standard 0.4× or 1× c-mount adapters.

The original light source, a halogen lamp, was substituted by a homemade passively cooled illuminator with high power LEDs of the type Luxeon M LXR7-SW65 (cold white, 6500 K) and LXR0-SR00 (royal blue, 450 nm, Philips Lumileds Lighting Company) for brightfield and fluorescence illumination, respectively. The light was collimated by an aspheric condenser lens (Edmund Optics) with a focal length of 13 mm. For fluorescence application the royal blue LED was used in combination with a bandpass excitation filter (448 nm, 20 nm bandwidth, OD6, Edmund Optics), a dichroic beam splitter (T470lpxr, 470 nm, Chroma) and a bandpass emission filter (520 nm, 70 nm bandwidth, OD6, Edmund Optics). This set of filters was chosen on the basis of the absorption and fluorescence spectra of isolated molecules of PTCDA (3,4,9,10-perylene tetracarboxylicacid dianhydride) adsorbed on KCl(100) terrace sites.[17] In this configuration, we measured a maximum light density of 250 mW/cm^2 at the position of the sample surface with the *Olympus* 40× objective.

D. Sample mounting and cooling

The construction of the sample mounting was optimized for low temperatures, good accessibility by surface science techniques, as for instance LEED and photoelectron spectroscopy, and compatibility with the light microscope. Especially the combination of low temperatures and good accessibility was challenging: On the one hand the sample needed good thermal

coupling to the cryostat, which is favored by short distances and large cross sectional areas; on the other hand it had to be in an exposed position for the approach of the front window of the microscope, without being hindered by the sample mounting or the cryostat. In addition, reduction of heat impact via cryoshields needed to be considered.

A detailed picture of the sample mounting and the cryoshield is shown in Fig. 2. The sample mounting consisted of three parts: A block made out of oxygen-free copper, two tungsten rods (3 mm in diameter) pressed into the copper block for optimal thermal contact and a sample holder made of solid silver pressed onto the tungsten rods. The Ag(100) sample was of the 'hat type' and had a diameter of 10 mm. It was fastened on top of the sample holder with a silver ring lid. Silver was used for the sample holder to avoid mechanical strain induced by differences in thermal expansion. As a further benefit, it has a high thermal conductivity. The crystal surface was positioned in the rotational axis of the manipulator, about 4 mm above the tungsten rods. In combination with the length of the rods (80 mm), this brought the sample in an exposed position with ideal accessibility for the microscope.

The copper block was pressed against a liquid helium cryostat by VAb GmbH that reached temperatures down to 5 K. Between the head of the cryostat and the copper block three 1.5 mm sapphire plates were inserted for electrical isolation. These sapphire plates also granted high heat conductance at low temperatures and thermal isolation at elevated sample temperatures required for annealing of the sample. Annealed 0.1 mm thick gold foil was inserted on both sides of the sapphire plates to compensate small irregularities of the fitted surfaces.

The sample could be heated by radiation from a 100 W tungsten filament at its rear side and by additional electron impact. Sample temperatures above 70 K were measured with a type K thermocouple attached to the sample holder. Cryogenic temperatures ($\leq$ 70 K) were measured via a silicon diode (DT-670B-SD, Lake Shore Cryotronics Inc.) mounted to the copper block. This location was apart from the sample, but is necessary since the Si-diode cannot withstand temperatures higher than 500 K. Despite that, an accurate temperature measurement was possible in the low temperature regime. This was checked by a calibration experiment with a second Si-diode mounted for test purposes directly to the rear side of the sample. We found that the temperature measured directly at the sample was less than 1 K above that measured on the copper block. For a reduced heat impact, Manganin cables were used to connect the Si-diode. All cables that were connected to the sample holder were precooled at the cryostat, as it is common.

We used a cryoshield made of polished aluminum. It was mounted to the second cooling stage of the cryostat, which was cooled by the helium backflow. As can be seen in Fig. 2, the cryoshield was composed of different parts in order to shield the entire sample mounting except the sample surface, which stuck out of the cryoshield and was the topmost surface for unrestricted access. The cryoshield was optimized for allowing inclined incidence or emission of probing beams (or particles) up to an angle of at least 45° with respect to the sample normal in all azimuthal directions.

The cooling was performed by either pumping or pressing liquid helium trough the cryostat. Usually the pumping method was used, because it was highly reproducible and the flux could easily be controlled especially in the case of small fluxes. However, we found this method to be limited by a minimum sample temperature of 12 K at a flux of 5 dm^3/h of liquid He. By pressing helium through the cryostat, sample temperatures of 6 K at a flux of 8 dm^3/h of liquid He could be achieved. This was done by applying about 400 mbar of extra He pressure to the Dewar.

III. Results and Discussion

A. Brightfield microscopy on a Ag(100) surface

The performance of the microscope is tested on a well prepared Ag(100) crystal. It represents a typical sample that has been used for surface science experiments for many years. It was extensively prepared by numerous cycles of Ar^+ ion sputtering with 1000 eV and subsequent annealing to 1000 K for one hour. It exhibits a shiny surface. Originally, the crystal was prepared by chemomechanical polishing. The crystal shows a very good and sharp low energy electron diffraction (LEED) pattern. As a measure for the microscopic crystal quality, the full width at half maximum $\Delta k_{\parallel}$ of the LEED spots is determined at an in-phase condition (81 eV) with respect to monoatomic Ag(100) steps. The corresponding length in real space $L = 2\pi/\Delta k_{\parallel}$ [18] has a value of ~600 Å. This can be considered to be a very good value for a metal crystal, since in general the limitations on *L* by the mosaic spread of metal samples are more pronounced.[19]

In the following, we show brightfield images of the crystal surface that were recorded with the *Nikon* 5× and 20× objectives, and with the *Olympus* 40× objective. We estimate that we achieve a resolution of 0.8 µm with the 40× objective, as these are the smallest features visible in our acquired images. Fig. 3(a) shows an overview image of the sample that was assembled from individual brightfield images. The contrast present in these images is related to the topology of the surface and originates in either specular or diffuse reflection of light. Unlike

the expectations that may have arisen from the diffraction data, the surface shows strong inhomogeneities and a macroscopic height corrugation. In addition, at some positions, the surface is damaged by scratches or contaminated by metal splinters that stick to the surface. On this length scale, no changes are observed after repeated cycles of sputtering and annealing. The corrugation is present on the entire sample surface; however, less and more corrugated regions can be identified. For example, near the edge of the crystal, the surface is slightly elevated with respect to the rest of the crystal and shows a very pronounced corrugation, whereas in the middle of the crystal smoother regions are more frequent.

A more detailed image of the surface is shown in Fig. 3(b). We find that the surface corrugation corresponds to a framework of flat areas that are surrounded by curved narrow protrusions. These are presumably macroscopic step bunches, which locally merge into each other. Additionally, at some positions also larger rather dot shaped protrusions can be observed. The width of the narrow protrusions along their short direction is always about 10 μm, their individual lengths vary and can exceed 200 μm depending on their location on the sample. Also the flat areas between them vary in size. They are 20 to 30 μm in diameter in the more corrugated and up to ~200 μm in the smoother regions of the surface.

The smallest structures that can be detected in brightfield mode are shown in Fig. 3(c). The image shows a close up of the above mentioned protrusions. On top and at the sides of the protrusions a ruffled substructure is observed. The size of the individual ruffles varies between 0.8 and 1.0 μm in diameter. In contrast, in the flat areas between the protrusions no additional substructure, such as the ruffles, can be detected. Thus, we conclude that the flat areas are the smoothest areas on the surface on this microscopic scale.

On this scale, further cycles of sputtering and annealing have only marginal influence on the images. We therefore assume that the formation or flattening of the corrugation is a rather slow process and the macroscopic morphology of the crystal surface changes rather on the scale of several tens of preparation cycles.

B. Fluorescence microscopy on monomers of PTCDA / KCl / Ag(100)

For the fluorescence imaging of adsorbed molecules an about 10 atomic monolayer thick KCl film was epitaxially grown on the Ag(100) crystal.[17] This film electronically decouples the dye molecules from the metallic Ag sample and prohibits quenching of the fluorescence.[20] The PTCDA coverage was varied between 1×10^{-5} and 5×10^{-2} of a complete monolayer.[21] Below 20 K sample temperature, the deposited PTCDA molecules are immobile and form a di-

luted phase. We are able to record fluorescence images for coverages above 1×10^{-3} of a monolayer. Below this concentration the fluorescence signal is too small and vanishes into a diffuse background signal that originates from residual excitation light surpassing the filters. This light is, different from the situation of fluorescence microscopy in solutions, reflected by the mirror like sample surface. In the brightfield images, neither signatures of the growth of the epitaxial KCl film, nor of the deposited PTCDA molecules can be detected.

Before we consider the details of the fluorescence images, we summarize some facts known about PTCDA on KCl from fluorescence spectroscopy: The molecules adsorb flat lying and azimuthally aligned to the KCl(100) surface on well-defined adsorption sites.[17, 22] As said above, the molecular surface diffusion of PTCDA is hampered below 20 K and thus attractive defect sites of the KCl surface, e.g., step edges, are not preferentially populated (different from the situation at higher temperatures). Also no aggregation into compact islands takes place.[23] The fluorescence spectra are dominated by a sharp 0-0 transition and show well resolved vibrational modes.[17] However, the quality of the fluorescence signal depends to some extend on the exact position of the excitation laser on the surface (diameter 200 μm), i.e. additional diffuse background signal or additional peaks from minor fluorescent species can be observed. Comparing these observations from spectroscopy experiments with the present results from brightfield microscopy these differences can tentatively be related to the local macroscopic quality of the sample surface. Spectra from generally smoother surface regions (cf. Fig. 3(a)) are proposed to give better quality than spectra taken from stronger corrugated or even defective regions.

In the fluorescence microscopy images, the averaged fluorescence intensity (integration area larger than 100×100 μm^2) is independent from the sample position, which corresponds to the fact that the deposition procedure leads to a homogeneous coverage. However, on the microscopic scale (see Fig. 4) the fluorescence signal is not constant, but shows structures with an additional contrast that increases with dye concentration. The image shown in Fig. 4(a) displays an overlay of a green colored fluorescence image with a brightfield image. It allows correlating the fluorescence contrast and the surface morphology. Two observations can be made: The first is a shading effect for the protruding structures. They have a brighter and a darker side. This is due to the inclined angle of incidence of the molecular beam (45° with respect to the surface normal). The protrusions are covered on the sides that face the evaporator; the opposite sides are shadowed and appear darker in fluorescence images. The second aspect is an additional contrast in the flat regions between the macroscopic protrusions (see

close-up in Fig. 4(b)). This contrast depends on the on the particular preparation of the sample, presumably on the preparation of the KCl-film. We see a dense pattern of brighter oval patches, about 5 μm in average diameter. Near the protrusions and on top of them they are elongated and their density increases, whereas in the smoother areas they are more roundish and clearly separated from each other. Between these oval patches the detected fluorescence intensity is not zero but noticeably smaller.

Up to now it is not fully understood, what causes this additional contrast in the fluorescence images. We can nevertheless exclude a relation to the concentration of PTCDA molecules on the surface, since the form and size of the patches does not change for increasing PTCDA concentrations. We estimate that at a coverage of 1×10^{-3} of a monolayer about 10^4 molecules contribute to a single patch of 20 μm^2. Consequently, a single molecule related contrast or random fluctuations of the molecule density can be excluded. Regarding the fact that the structure of the fluorescence contrast is correlated to the morphology of the surface, it is more likely that additional morphologic effects of the surface or the epitaxial KCl film are decisive here. One explanation is, e.g., based on a further corrugation of the Ag surface that is not seen in brightfield mode due to a lack of contrast. Corrugations on this length scale (5 μm) were reported for example by *Cheynis et al.*. They observed a morphology of a Au(111) surface with plateau- and canyon-like structures in LEEM images.[24] Possibly the KCl film is also inhomogeneous and surface areas remain un-wetted by the KCl, preferentially where canyon-like structures are present. There, the PTCDA molecules are adsorbed to the bare silver surface where their fluorescence is quenched. In conclusion, we propose that in these images the fluorescence contrast is related to the inhomogeneities in the KCl film.

Finally, in Fig. 4(c) we show a fluorescence image of a larger dot shaped protrusion in order to demonstrate the achieved resolution. As can be seen, it is covered and surrounded by small bright spots that have a diameter of about 0.7 μm. The origin of these spots is not clear, yet. They could be related to cluster formation of molecules or emission from defect sites. A reliable explanation and assignment of these is however out of reach of the present work and asks for a combination of spatial and spectral resolution.

IV. Summary

We demonstrated the operation of an epi-illumination light microscope adapted to an UHV chamber by recording brightfield images of a well prepared Ag(100) surface used for surface science experiments. We could resolve a surface morphology with regular corrugations in

height on a lateral scale of 10 – 200 µm. Fluorescence images of diluted dye molecules deposited and imaged at 6 K on a thin KCl film show a pattern of structures on the scale of 2 – 10 µm, which we attribute to inhomogeneous "wetting" of the surface by the KCl film. We propose that this type of UHV light microscope is a helpful tool to identify well-suited surface positions for experiments with other techniques or to study the growth of deposits on the µm scale, e.g. for organic semiconductors. A combination with spectroscopic resolution also appears possible.

Acknowledgements

We thank Peter Koll for manufacturing the metal glass joint and the associated glass tube. The project was supported by the Deutsche Forschungsgemeinschaft under the project SO407/8-1.

References

[1]G. Binnig, H. Rohrer, C. Gerber and E. Weibel, Phys. Rev. Lett. **49**, 57 (1982).

[2]G. Binnig, C. F. Quate and C. Gerber, Phys. Rev. Lett. **56**, 930 (1986).

[3]E. Bauer, Rep. Prog. Phys. **57**, 895 (1994).

[4]H. H. Rotermund, Surf. Sci. **283**, 87 (1993).

[5]F. J. Giessibl, Science **267**, 68 (1995).

[6]E. Bauer, M. Mundschau, W. Swiech and W. Telieps, Ultramicroscopy **31**, 49 (1989).

[7]O. H. Griffith and G. F. Rempfer, Ultramicroscopy **24**, 299 (1988).

[8]M. L. Blumenfeld, B. S. Tackett, L. K. Schirra, J. M. Tyler and O. L. A. Monti, Revi. Sci. Instr. **80**, 103101 (2009).

[9]L. K. Schirra, B. S. Tackett, M. L. Blumenfeld and O. L. A. Monti, J. Chem. Phys. **131**, 124702 (2009).

[10]B. Sick, B. Hecht and L. Novotny, Phys. Rev. Lett. **85**, 4482 (2000).

[11]J. J. Macklin, J. K. Trautman, T. D. Harris and L. E. Brus, Science **272**, 255 (1996).

[12]D. A. Neuhaus, Angew. Chem. **64**, 158 (1952).

[13]A. H. Schäfer, C. Seidel and H. Fuchs, Thin Solid Films **379**, 176 (2000).

[14]L. Kankate, F. Balzer, H. Niehus and H. G. Rubahn, Thin Solid Films **518**, 130 (2009).

[15]F. Balzer and H. G. Rubahn, Adv. Funct. Mater. **15**, 17 (2005).

[16]A. Köhler, J. R. Microsc. Soc. **14**, 261 (1894).

[17]M. Müller, A. Paulheim, C. Marquardt and M. Sokolowski, J. Chem. Phys. **138**, 064703 (2013).

[18]M. Horn-von Hoegen, Z. Kristallogr. **214**, 591 (1999).

[19]M. Sokolowski and H. Pfnür, Phys. Rev. B **49**, 7716 (1994).

[20]W. Gebauer, A. Langner, M. Schneider, M. Sokolowski and E. Umbach, Phys. Rev. B **69**, 155431 (2004).

[21]M. Müller, A. Paulheim, A. Eisfeld and M. Sokolowski, J. Chem. Phys. **139**, 044302 (2013).

[22]Q. Guo, A. Paulheim, M. Sokolowski, H. Aldahhak, E. Rauls and W. G. Schmidt, J. Phys. Chem. C **118**, 29911 (2014).

[23]A. Paulheim, M. Müller, C. Marquardt and M. Sokolowski, Phys. Chem. Chem. Phys. **15**, 4906 (2013).

[24]F. Cheynis, F. Leroy, A. Ranguis, B. Detailleur, P. Bindzi, C. Veit, W. Bon and P. Müller, Rev. Sci. Instr. **85**, 043705 (2014).

Figure Captions

Fig. 1: Overview of the epi-illumination light microscope including the optical components, the sample holder and the glass head. The optical pathways corresponding to the conjugated field and aperture planes are sketched in red and yellow, respectively. The trinucular head and the camera are not drawn to scale. For further details see text.

Fig. 2: Schematic drawing of the sample mounting (top) and the cryoshield (bottom). For further details see text.

Fig. 3: Brightfield images of the Ag(100) crystal surface. (a) Overview image of the sample. The image was assembled from individual pictures that were taken with a 5× objective and a 1× c-mount adapter. To avoid artifacts from the image plane curvature the individual images were taken with a reduced field of view. The sample shows macroscopic defects like scratches and splinters and has a macroscopic corrugation. (b) Enlarged brightfield image of the surface corrugation (objective 20×, c-mount 0.4×). The surface shows a dense network of curved linear protrusions with flat areas in between. (c) Detail image of the linear protrusions with additional substructure (objective 40×, c-mount 1×).

Fig. 4: Fluorescence images of diluted PTCDA molecules (1% of a monolayer) on a 10 monolayer thick KCl-film on Ag(100) at T = 6 K. (a) Superposition of a brightfield image and a green colored fluorescence image (objective 20×, c-mount 0.4×, exposure time 0.5 s). The white arrow indicates the azimuthal direction of the molecular deposition, which leads to a shading of the surface protrusions. (b) Magnification of the fluorescence image of the white box in (a). The fluorescence images show an additional structured contrast in the flat surface areas. We attribute this to partial open regions in the KCl film (For better visibility, a background signal was subtracted). (c) Detailed fluorescence image of a single dot shaped protrusion on the surface demonstrating the shading effect and the achieved resolution (objective 40×, c-mount 1×, exposure time 2 s). In contrast to (b) the surface shows no additional structured contrast, but small bright spots on top and around the macroscopic defect. For further details see text.

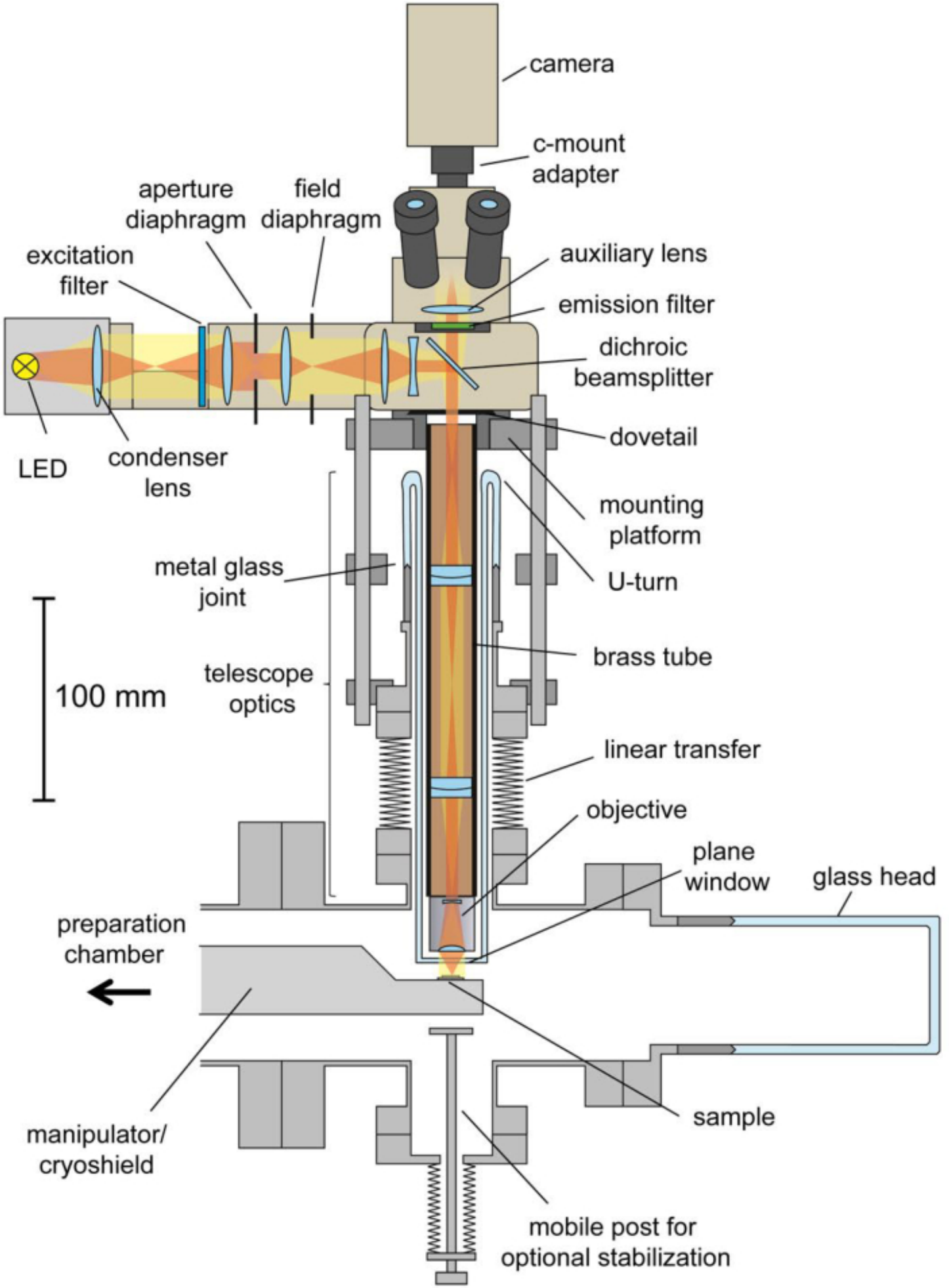
camera
c-mount adapter
aperture diaphragm
field diaphragm
excitation filter
auxiliary lens
emission filter
dichroic beamsplitter
dovetail
LED
condenser lens
mounting platform
metal glass joint
U-turn
brass tube
telescope optics
100 mm
linear transfer
objective
plane window
glass head
preparation chamber
manipulator/ cryoshield
sample
mobile post for optional stabilization

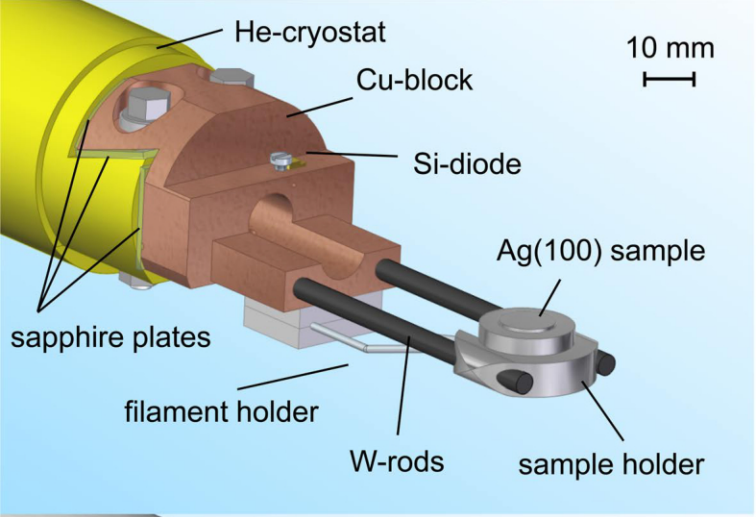
He-cryostat
10 mm
Cu-block
Si-diode
Ag(100) sample
sapphire plates
filament holder
W-rods
sample holder

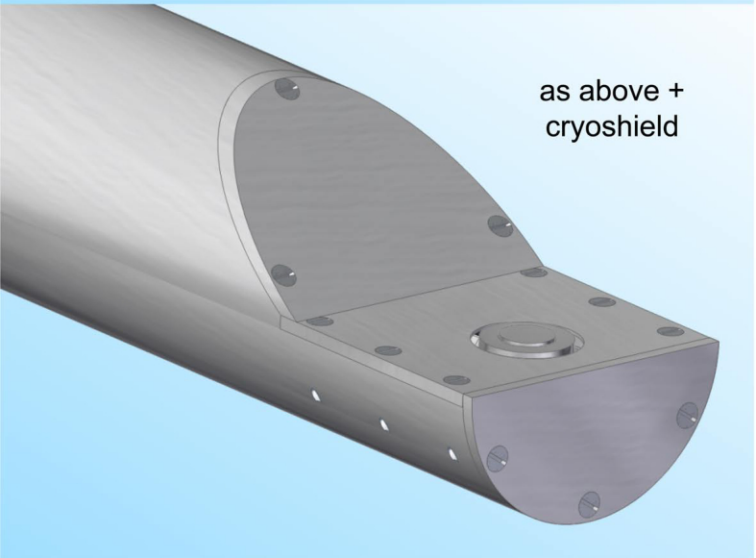
as above +
cryoshield

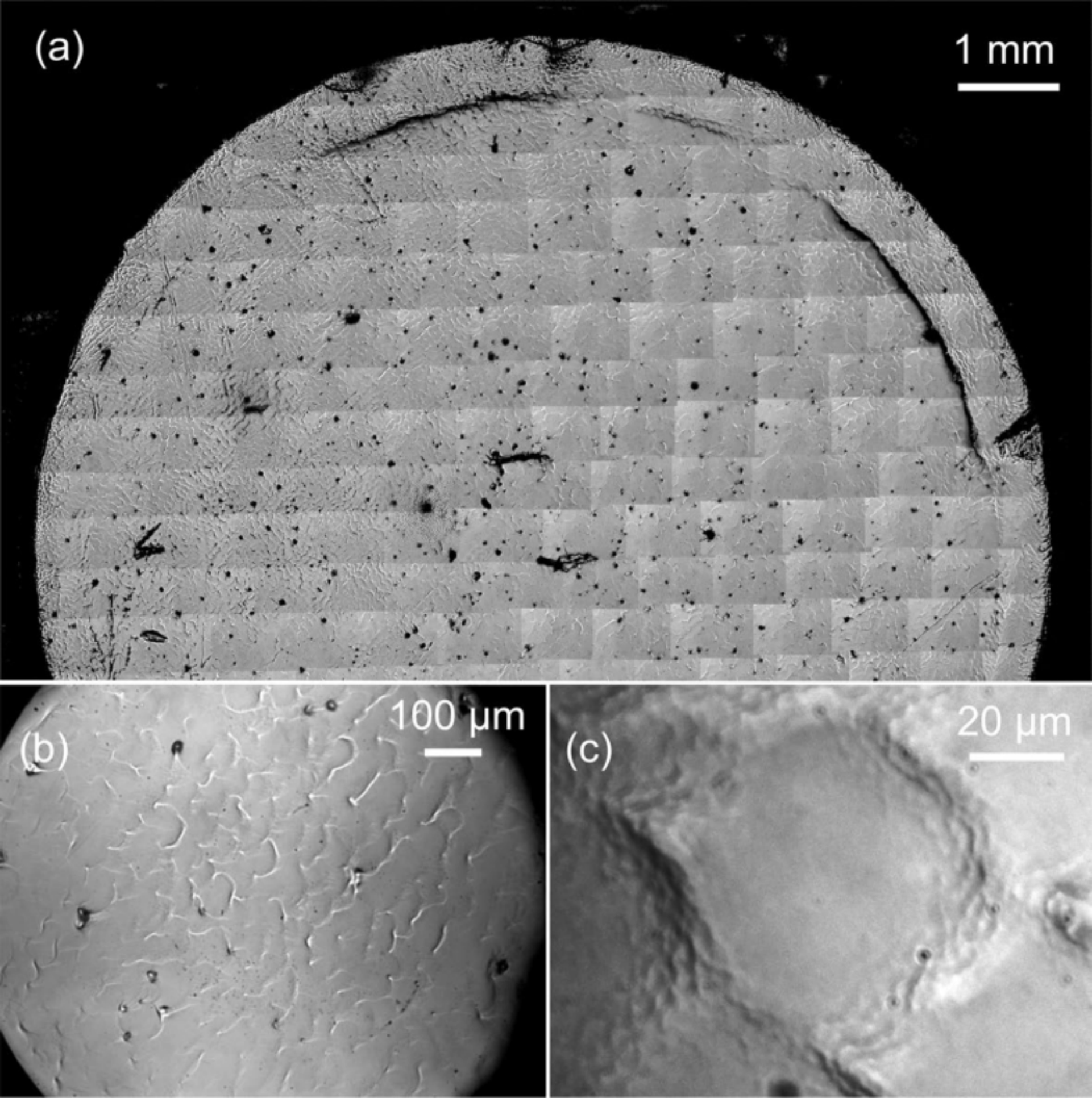
(a)
1 mm
(b)
100 µm
(c)
20 µm

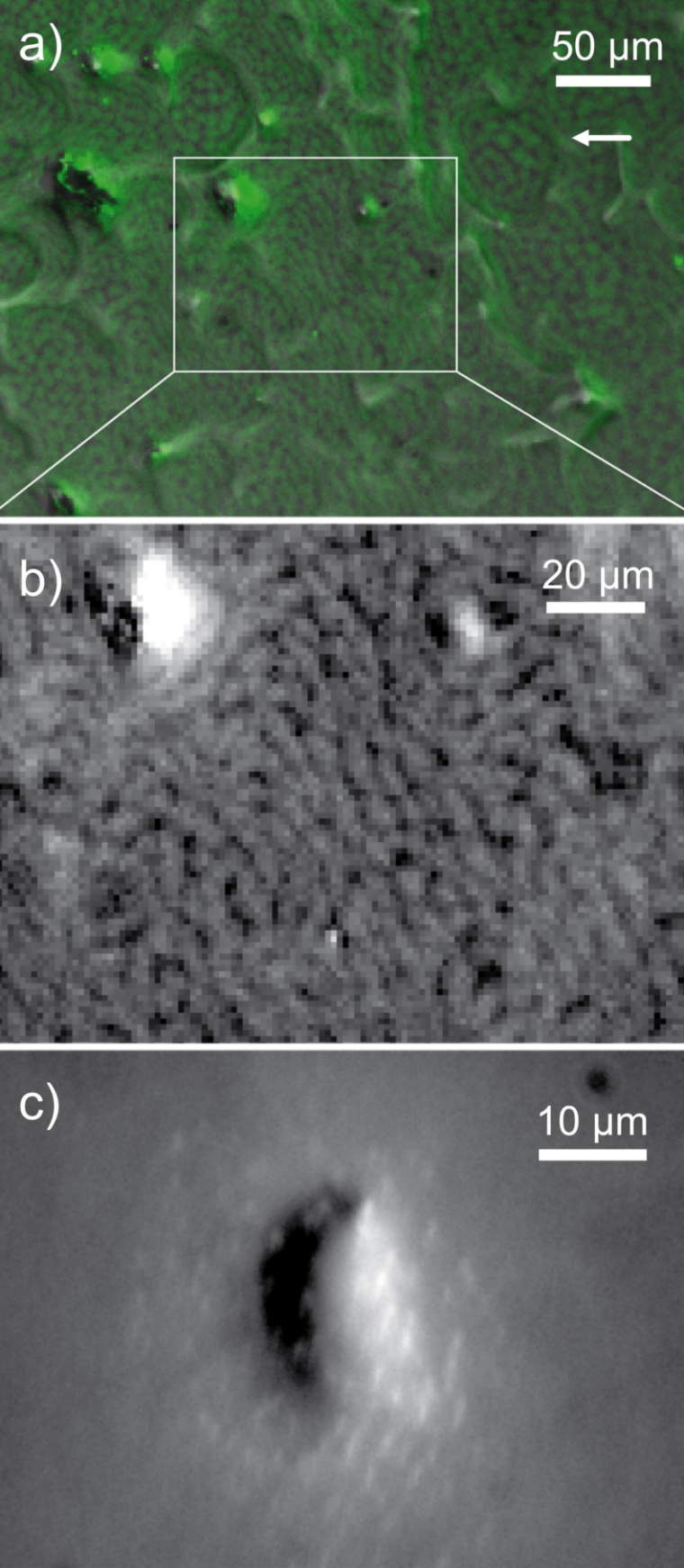
a)
50 µm
b)
20 µm
c)
10 µm